

Comparison of MR-guided radiotherapy accumulated doses for central lung tumors with non-adaptive and online adaptive proton therapy

Moritz Rabe¹  | Miguel A. Palacios² | John R. van Sörnsen de Koste² |
 Chukwuka Eze¹  | Martin Hillbrand³ | Claus Belka^{1,4} | Guillaume Landry¹ |
 Suresh Senan²  | Christopher Kurz¹

¹Department of Radiation Oncology, University Hospital, LMU Munich, Munich, Germany

²Department of Radiation Oncology, Amsterdam University Medical Centers, location VUmc, Amsterdam, The Netherlands

³Institut für Radio-Onkologie, Kantonsspital Graubünden, Chur, Switzerland

⁴German Cancer Consortium (DKTK), Partner Site Munich, Munich, Germany

Correspondence

Moritz Rabe, Department of Radiation Oncology, University Hospital, LMU Munich, 81377 Munich, Germany.
 Email: moritz.rabe@med.uni-muenchen.de

Suresh Senan and Christopher Kurz share last authorship.

Abstract

Background: Stereotactic body radiation therapy (SBRT) of central lung tumors with photon or proton therapy has a risk of increased toxicity. Treatment planning studies comparing accumulated doses for state-of-the-art treatment techniques, such as MR-guided radiotherapy (MRgRT) and intensity modulated proton therapy (IMPT), are currently lacking.

Purpose: We conducted a comparison of accumulated doses for MRgRT, robustly optimized non-adaptive IMPT, and online adaptive IMPT for central lung tumors. A special focus was set on analyzing the accumulated doses to the bronchial tree, a parameter linked to high-grade toxicities.

Methods: Data of 18 early-stage central lung tumor patients, treated at a 0.35 T MR-linac in eight or five fractions, were analyzed. Three gated treatment scenarios were compared: (S1) online adaptive MRgRT, (S2) non-adaptive IMPT, and (S3) online adaptive IMPT. The treatment plans were recalculated or reoptimized on the daily imaging data acquired during MRgRT, and accumulated over all treatment fractions. Accumulated dose-volume histogram (DVH) parameters of the gross tumor volume (GTV), lung, heart, and organs-at-risk (OARs) within 2 cm of the planning target volume (PTV) were extracted for each scenario and compared in Wilcoxon signed-rank tests between S1 & S2, and S1 & S3.

Results: The accumulated GTV $D_{98\%}$ was above the prescribed dose for all patients and scenarios. Significant reductions ($p < 0.05$) of the mean ipsilateral lung dose (S2: -8%; S3: -23%) and mean heart dose (S2: -79%; S3: -83%) were observed for both proton scenarios compared to S1. The bronchial tree $D_{0.1cc}$ was significantly lower for S3 (S1: 48.1 Gy; S3: 39.2 Gy; $p = 0.005$), but not significantly different for S2 (S2: 45.0 Gy; $p = 0.094$), compared to S1. The $D_{0.1cc}$ for S2 and S3 compared to S1 was significantly ($p < 0.05$) smaller for OARs within 1–2 cm of the PTV (S1: 30.2 Gy; S2: 24.6 Gy; S3: 23.1 Gy), but not significantly different for OARs within 1 cm of the PTV.

Conclusions: A significant dose sparing potential of non-adaptive and online adaptive proton therapy compared to MRgRT for OARs in close, but not direct proximity of central lung tumors was identified. The near-maximum dose to the bronchial tree was not significantly different for MRgRT and non-adaptive IMPT.

This is an open access article under the terms of the [Creative Commons Attribution](https://creativecommons.org/licenses/by/4.0/) License, which permits use, distribution and reproduction in any medium, provided the original work is properly cited.

© 2023 The Authors. *Medical Physics* published by Wiley Periodicals LLC on behalf of American Association of Physicists in Medicine.

Online adaptive IMPT achieved significantly lower doses to the bronchial tree compared to MRgRT.

KEYWORDS

bronchial tree, central lung tumor, dose accumulation, MR-linac, online adaptive proton therapy

1 | INTRODUCTION

Early-stage central lung tumors are currently treated with both stereotactic body radiation therapy (SBRT)^{1–5} and proton therapy.^{6–9} Clinical trials comparing both modalities are missing in the literature.¹⁰ The lack of online plan adaptation for proton therapy is recognized as a limitation that hinders further clinical adoption of proton therapy for this entity,^{10,11} especially since the clinical introduction of magnetic resonance imaging-guided radiotherapy (MRgRT) with MR-linacs.^{12,13} MRgRT offers high soft tissue contrast, daily online plan adaptation and real-time imaging-based gated beam delivery.^{14–17} Stereotactic MRgRT of central and ultracentral lung tumors has now been clinically established,^{18–21} and early reports suggest high local control rates and low rates of treatment-related high-grade toxicities.^{18,21} MRgRT has the potential for a reduction of the maximum dose to the proximal bronchial tree (PBT) and PBT sub-volumes exposed to high doses. These parameters have been linked to high-grade toxicity and treatment-related deaths.^{1,5,22–24}

Robust treatment plan optimization is commonly used in proton therapy clinical practice today to prospectively account for potential interfractional changes and range uncertainties.²⁵ A few clinics have implemented protocols for offline adaptive proton therapy based on additional computed tomography (CT) scans acquired over the course of treatment to better mitigate the potentially adverse effects on the dose distributions caused by interfractional changes.^{26,27} While this approach can improve the target coverage and sparing of OARs, the adaptation process is slow and anatomical or physiological changes occurring on time scales of minutes or hours cannot be accounted for.²⁸

Online adaptive proton therapy, in which the treatment plan is adapted and reoptimized based on the observed daily anatomy in treatment position, is being discussed as a future method to minimize treatment-related uncertainties caused by interfractional changes. However, this technique is not clinically employed, yet.^{28,29} Online adaptive proton therapy will require daily volumetric imaging data of the patient in treatment position, which could be acquired through in-room CT, cone-beam CT (CBCT), or magnetic resonance imaging (MRI). In-room CT scanners are already installed at a few proton therapy centers.^{11,30–32} Also CBCT scanners are becoming more widespread in proton therapy facilities,¹¹ and several methods to correct the acquired CBCT images

for artifacts and rescale the image intensities to allow accurate dose calculations have been proposed in the literature.^{33–35} MR-guided proton therapy is a promising future treatment modality,^{36–39} and first prototype systems have been constructed.⁴⁰ Several technological and methodological advancements that are additionally required for the clinical implementation of online adaptive proton therapy have been achieved in the last decade. This includes virtual and synthetic CT generation methods,^{41,42} tools to support daily in-room image segmentation,⁴³ fast dose calculation and reoptimization approaches, and tools and concepts for online quality assurance.^{28,29,36}

The promising prospect of the clinical introduction of online adaptive proton therapy raises the question whether radiotherapy of central lung tumors – where the target is located in close proximity to radiosensitive OARs – could be improved with respect to current state-of-the-art proton therapy and the online adaptive gated treatments at MR-linacs already available today. Therefore, the purpose of this study was to quantify potential differences from interfractional changes in accumulated doses between MRgRT, today's state-of-the-art robustly optimized gated IMPT, and online adaptive gated IMPT for central lung tumors. We performed a retrospective planning and dose accumulation study with imaging data acquired during MRgRT at an MR-linac. A special focus was set on analyzing the accumulated doses to the PBT.

2 | METHODS AND MATERIALS

2.1 | Patient characteristics

This retrospective study was approved by the institutional medical ethics committee of the Amsterdam University Medical Centers (AUMC) (reference number 2018.602). Eighteen patients (median age: 70 years; range: 40–79 years) with early-stage central lung tumors treated at a 0.35 T MRIdian MR-linac (ViewRay Inc., Oakwood Village, OH, USA)^{16,44} at the Department of Radiation Oncology at AUMC between April 2018 and January 2020 were included in the study. Patient and treatment characteristics are summarized in Table 1 and patient-specific information is listed in Table S1. All patients had a GTV located within 2 cm of any mediastinal critical structure, including the PBT, esophagus, heart, major vessels, and the spinal cord.^{4,45}

TABLE 1 Patient and treatment characteristics.

Patient and treatment characteristics	
Sex	
Male	11 (61%)
Female	7 (39%)
Age ^a ; median (range) in years	70 (40–79)
GTV location	
Moderately central	13 (72%)
Paracardial	4 (22%)
Ultracentral	0 (0%)
Other	1 (6%)
Fractionation	
8 × 7.5 Gy	13 (72%)
5 × 11 Gy	5 (28%)
GTV size ^a ; mean (range) in cm ³	17.5 (0.4–59.9)
Number of OARs within 2 cm of PTV	
1	1 (6%)
2	8 (44%)
3	6 (33%)
4	2 (11%)
5	1 (6%)
Proximal bronchial tree within 1 cm of GTV	
Yes	10 (56%)
No	8 (44%)

^aAt time of initial treatment planning.

Depending on the PTV location, the cases were categorized as moderately central ($n = 13$; PTV within 2 cm of the PBT) or paracardial ($n = 4$; distance between PTV and PBT ≥ 2 cm; PTV overlapping with mediastinal or paracardial pleura).¹⁹ One case did not fall in either category (aorta within 2 cm of PTV without overlap; distance to PBT ≥ 2 cm). No ultracentral lung tumors (PTV overlapping the trachea or main bronchi) were included.⁴⁶

Treatment planning and dose accumulation were performed for three treatment scenarios: (S1) online adaptive gated MRgRT, (S2) non-adaptive gated IMPT, and (S3) online adaptive gated IMPT. An overview of the treatment planning specifics and dose accumulation steps is given in Table 2.

2.2 | MRgRT (S1)

Two fractionation schemes of 8×7.5 Gy ($n = 13$) and 5×11 Gy ($n = 5$) were applied, corresponding to a total physical dose of 60 Gy and 55 Gy, respectively. Treatment planning, plan adaptation, and delivery with stereotactic online adaptive gated MRgRT was performed as previously described.^{14,18,47} Briefly summarized, a breath-hold CT image and MRI scan (bSSFP

sequence; resolution: $1.6 \times 1.6 \times 3.0$ mm³; acquisition time: 17 s) at the MR-linac were acquired for treatment planning. Contouring was performed on the planning MRI scan. The dose was calculated on a virtual CT (vCT) image, generated by propagating the CT values of the planning CT image to the planning MRI scan using deformable image registration (DIR).⁴⁴

A step-and-shoot intensity-modulated radiotherapy (IMRT) baseline plan with 6 MV flattening filter-free photons was created with the MRIdian planning system. The dose was calculated on an isotropic 2 mm dose grid⁴⁸ with a Monte Carlo algorithm with statistical uncertainty of 1%. The GTV was isotropically expanded by 5 mm to form the PTV. The plans were optimized to achieve 95% PTV coverage by the prescribed dose (PTV $V_{100\%} \geq 95\%$) while minimizing doses to OARs in proximity to the PTV.¹⁹ The OAR constraints used to set up the planning objectives are listed in Table S2.

On each day of treatment, an MRI scan was first acquired. Target and OAR contours were propagated from the planning to the fractional MRI scan using DIR, followed by manual corrections. A corresponding vCT image was automatically created based on the planning vCT image and the deformation vector fields (DVF) of the same DIR. The baseline plan was recalculated on this vCT image. The baseline treatment plan was reoptimized using the same beam angles and planning objectives if clinical criteria of the recalculated baseline plan were not met. The clinician then selected the original or adapted plan for treatment delivery.^{18,19}

Gated treatment delivery was performed during shallow-inspiration breath-holds based on real-time 2D cine MRI in sagittal orientation at a frame rate of 4 Hz, as previously described.^{14,47} The gating window was defined as the GTV contour in a preselected sagittal slice, expanded isotropically by 3 mm.

All patient data acquired over the course of MRgRT treatment were exported in DICOM format for offline analysis. Each patient dataset consisted of: planning MRI scan with delineations, fractional MRI scans with delineations, corresponding planning vCT image and fractional vCT images, baseline plan dose distribution, and fractional dose distributions of the delivered treatment plans.

2.3 | Proton therapy planning

Proton therapy planning for scenarios S2 and S3 was performed with a research version of the treatment planning system (TPS) RayStation 10B (version 10.1.100.0; RaySearch Laboratories, Stockholm, Sweden). All data exported from the MRIdian system were imported into the research TPS. All fractional MRI scans and corresponding vCT images were already rigidly registered as during treatment delivery in S1. After export from the MRIdian system, the planning MRI scan and vCT image

TABLE 2 Overview of treatment planning scenarios.

Treatment scenario	S1	S2	S3
Description	MR-guided SBRT	State-of-the-art non-adaptive IMPT	Online adaptive IMPT
Treatment modality	Photons	Protons	Protons
Gating	Yes	Yes	Yes
Daily plan adaptation	Yes	No	Yes
Margin concept	PTV = GTV + 5 mm	ITV = GTV + 3 mm with density override	ITV = GTV + 3 mm with density override
Robustness settings	n/a	6 mm position/3% range	2 mm position/3% range
TPS used for plan generation	MRIdian TPS	RayStation	RayStation
Dose grid used for plan optimization	2 mm isotropic	2 mm isotropic	2 mm isotropic
Dose engine	Monte Carlo (1% statistical uncertainty)	Monte Carlo (1% statistical uncertainty)	Monte Carlo (1% statistical uncertainty)
Dosimetric evaluation in RayStation	<ul style="list-style-type: none"> • Import of fractional doses • Deformation of fractional doses to baseline MRI • Dose accumulation on baseline MRI 	<ul style="list-style-type: none"> • Recalculation of baseline plan on baseline vCT (without density override) • Normalization of baseline plan to GTV $D_{98\%}$ in S1 baseline plan • Recalculation of baseline plan on fractional vCT (without density override) • Deformation of fractional doses to baseline vCT • Dose accumulation on baseline vCT 	<ul style="list-style-type: none"> • Recalculation of adapted plans on fractional vCT (without density override) • Normalization of adapted plans to GTV $D_{98\%}$ in S1 adapted plans • Deformation of fractional doses to baseline vCT • Dose accumulation on baseline vCT

Note: Further details are provided in the main text.

Abbreviations: TPS, treatment planning system; vCT, virtual CT.

were not registered to the fractional imaging data. Therefore, the planning MRI scan was first rigidly registered to the MRI scan of the first fraction, focused on the GTV and discarding rotations. The resulting translation vector was applied to the planning vCT image to register it with the fractional vCT images.

The same fractionation schemes as for S1 were used. For both S2 and S3, IMPT plans were created using a generic machine model representing a cyclotron with pencil beam scanning delivery (available energy range: 70–230 MeV; nominal spot size (1σ) at isocenter: 7.0 mm (70 MeV)/2.7 mm (230 MeV); Bragg peak width at 80% dose level: 1.7 mm (70 MeV)/8.5 mm (230 MeV); hexagonal spot scanning pattern with automatic spot spacing of 1.06 times 1σ of the lateral Bragg peak spread; automatic energy layer spacing corresponding to the width at 80% dose level of the more distant Bragg peak). A constant relative biological effectiveness (RBE) factor of 1.1 was applied to scale the physical dose. All plans were optimized on the planning vCT image (S2 and S3) or fractional vCT images (only S3) with the same delineations as used during MRgRT on an isotropic 2 mm dose grid, with a Monte Carlo algorithm with statistical uncertainty of 1%. For each treatment plan, three coplanar beam directions were selected depending on the location of OARs in proximity to the GTV (see Table S1 for a patient-specific list of beam directions). A range

shifter with a water equivalent thickness of 4 cm was added if needed. The same OAR constraints as used in S1 (Table S2) were considered during planning for S2 and S3.

Both S2 and S3 assumed accurate GTV-focused patient positioning based on volumetric image guidance modalities and gated beam delivery. These assumptions were made, since CBCT scanners are increasingly available at proton therapy centers^{11,28} and respiratory-gated pencil beam scanning for proton therapy has been clinically implemented by several proton centers in the last years.^{49–52} Setup and range uncertainties were accounted for by robust optimization. Daily plan adaptations were only performed for S3, hence, different robustness settings were used for S2 and S3, as detailed below. Intrafractional changes of the target, that is, the residual motion of the GTV within the gating window, were accounted for by the creation of an internal target volume (ITV), as described below.

2.4 | Non-adaptive IMPT (S2)

S2 mimicked state-of-the-art IMPT treatments with volumetric image guidance and gated beam delivery, but without plan adaptations. Thus, only a baseline treatment plan was created on the planning vCT image. The

ITV in proton therapy is often defined as the union of the GTV in a few breathing phases around the chosen gating phase, as observed on a 4D-CT scan.^{49,53} No 4D-CT scan was acquired for MRgRT. Therefore, the ITV in S2 (equivalent to the gating window) was defined as a 3 mm uniform expansion of the GTV instead (i.e., identical to the definition in S1), which was overridden with muscle tissue density (mass density: $\rho = 1.05 \text{ g/cm}^3$) during plan optimization.⁵⁴ Robustness settings of 6 mm isotropic positional uncertainty and 3% density uncertainty were applied for the target and OARs for plan optimization (total number of considered scenarios: 45; Table S3) to account for interfractional anatomical changes, setup, and range uncertainties, as per a published clinical protocol.⁵⁴

The optimized baseline plan was recalculated on the planning vCT image without ITV density override. Subsequently, the S2 baseline plan was normalized to the same GTV $D_{98\%}$ as in the baseline plan of S1. Plan normalization was performed to enable a fair comparison of OAR doses between the two treatment scenarios by matching the planned target doses.

For dose accumulation, the final rescaled baseline plan was recalculated on the vCT images of each fraction without ITV density override. Depending on the fractionation scheme, this resulted in 5 or 8 fractional dose distributions per patient.

2.5 | Online adaptive IMPT (S3)

S3 mimicked future in-room imaging-based online adaptive gated IMPT. First, a baseline treatment plan was generated on the planning vCT image using the same beam angles and range shifter as for S2. Equivalent to S2, an ITV (GTV + 3 mm) with muscle tissue density override was created for treatment planning. Robustness settings of 2 mm isotropic positional uncertainty and 3% density uncertainty were applied for the target and OARs (total number of considered scenarios: 21; Table S3). The value of 2 mm was chosen to account for residual setup and geometric uncertainties, as an equivalent for the 2 mm margin between the boundaries of the gating window and PTV in S1.

The baseline plan was then adapted on the fractional vCT images (including ITV with density override), using the same beam angles, range shifters, planning objectives, and robustness settings as for the baseline plan. The plan adaptation process was automated by exploiting the Python scripting capabilities of the research TPS. The adapted plans were recalculated on the corresponding fractional vCT images without ITV density override, again resulting in 5 or 8 fractional dose distributions per patient available for dose accumulation. The resulting fractional dose distributions were normalized by rescaling the S3 adapted plans to the same GTV $D_{98\%}$ as the adapted plans for each fraction for S1.

2.6 | Dose accumulation

Dose accumulation for all treatment scenarios was performed with the research TPS. Each fractional MRI scan was deformably registered to the planning MRI scan. The hybrid intensity and structure based ANatomically CONstrained Deformation Algorithm (ANACONDA)⁵⁵ implemented in the research TPS was used, setting the planning MRI scan as fixed and the fractional MRI scan as moving image. The objective function of the ANACONDA algorithm includes an image similarity term (with the correlation coefficient as similarity metric), regularization terms, and a penalty term that penalizes surface distance between so-called controlling regions of interest (ROIs) in the fixed and moving images, to combine image intensity information and shape-based information. In the research TPS, additional focus ROIs can be defined, to focus the DIR on specific image regions.

We set the contoured lungs, GTV, PTV, and all contoured OAR structures within the thorax as focus ROIs, and the GTV as controlling ROI for all DIRs. The goal of this approach was to achieve the highest DIR accuracy in the target region since the dose parameter analyses were primarily focused on high doses delivered to this volume. The DIRs were optimized semi-automatically using Python scripts within the research TPS's scripting environment. The results were visually assessed with overlay plots for several randomly selected DIRs per patient, with particular attention on the target region. The resulting DVFs were copied to the fractional vCT images to deformably register them to the planning vCT image.

Subsequently, for S1, all fractional delivered dose distributions were mapped to the planning MRI scan using the corresponding DVFs. For S2 and S3, all recalculated dose distribution on the fractional vCT images (without density override) were mapped to the planning vCT image with the same DVFs. Finally, all mapped dose distributions on the planning MRI scan (S1) and planning vCT image (S2 & S3) were summed to create one accumulated dose distribution per treatment scenario and patient.

When interfractional changes such as tumor shrinkage introduce dissimilarities between images, DIR may deliver inaccurate and anatomically incorrect results.⁵⁶ To quantify these changes and estimate their impact on the dose accumulation accuracy, the GTV size was determined on each fractional MRI scan and compared to its initial volume on the planning MRI scan.

2.7 | Dose parameter analysis

For each patient and accumulated dose for each scenario, the constraints listed in Table S2 were checked for fulfillment. Only constraints for OARs located within 2 cm

of the PTV were considered. The total number of applicable and fulfilled constraints was calculated for each scenario and compared.

The following dose-volume histogram (DVH) parameters were retrieved from the accumulated dose distributions for each patient and treatment scenario, using the original delineations defined on the planning MRI scan for initial treatment planning during MRgRT: GTV $D_{98\%}$, mean GTV dose (D_{mean}), GTV $D_{2\%}$, mean dose to the ipsilateral lung (excluding GTV), mean heart dose, and near-maximum doses ($D_{0.1\text{cc}}$) to OARs located within 2 cm of the PTV (defined for S1).⁵⁷ The following OARs were considered: heart, PBT, chest wall, great vessels, esophagus, spinal cord, and trachea (see Table S1 for a patient-specific list of considered OARs). The $D_{0.1\text{cc}}$ values for each of these OARs separately, for all OARs with a distance ≤ 1 cm to the PTV pooled, and all OARs with a distance between 1 and 2 cm to the PTV pooled were considered for statistical analysis. Furthermore, for patients with a PTV within 2 cm of the PBT, the absolute volumes of the PBT receiving 100%, 80%, 60%, 40%, and 20% of the prescribed dose ($V_{100\%}$, $V_{80\%}$, $V_{60\%}$, $V_{40\%}$, and $V_{20\%}$) were analyzed.

2.8 | Statistical analysis

Pairwise comparisons of the DVH parameters with at least six cases ($n \geq 6$) were performed between S1 and S2, and between S1 and S3, respectively, with a two-tailed Wilcoxon signed-rank test. Additionally, the DVH parameters of OARs with a low number of cases ($n < 6$) were pooled before statistical testing. All tests were performed with Python (version 3.6.5) using the implementation of the Wilcoxon signed rank test in the package `scipy` (`scipy.stats.wilcoxon`; version 1.5.4). A p -value < 0.05 was considered to be statistically significant.

3 | RESULTS

3.1 | Interfractional GTV changes

The median GTV size at time of treatment planning was 8.8 cm^3 (range: $0.4\text{--}59.9 \text{ cm}^3$). The median (5th percentile, 95th percentile) absolute changes between the GTV on all fractional MRI scans with respect to the planning MRI scans was $+0.3 \text{ cm}^3$ (-0.4 cm^3 , $+3.8 \text{ cm}^3$). These changes were below $\pm 1 \text{ cm}^3$ in 69% of cases.

3.2 | Dose parameter analysis

Figure 1 depicts the accumulated dose distributions and the respective DVHs for an exemplary patient for the

three treatment scenarios. For this patient, the accumulated GTV $D_{98\%}$ was similar for S1 (64.7 Gy) and S3 (64.6 Gy), but slightly larger for S2 (66.4 Gy). Due to the overlap of the bronchial tree with the target volumes, the $D_{0.1\text{cc}}$ was comparable in all three scenarios while the bronchial tree volume at low dose levels was considerably lower for the proton therapy scenarios S2 and S3.

A total of 60, 65, and 69 out of 87 applicable constraints were fulfilled by the accumulated dose distributions for S1, S2, and S3, respectively. The most frequently violated constraints were the $D_{0.1\text{cc}}$ constraints for the chest wall (violated in 6, 9, and 7 cases for S1, S2, and S3, respectively), PBT (9, 8, and 4 cases), and heart (3, 3, and 5 cases). While the number of violated $D_{0.1\text{cc}}$ constraints was comparable for the three scenarios (18, 20, and 16 cases), the number of violated volume constraints was considerably smaller for the two proton therapy scenarios (9, 2, and 2 cases).

The dose parameter results are summarized in Table 3. For all patients and treatment scenarios, the accumulated GTV $D_{98\%}$ was above the prescribed dose of 60 Gy ($8 \times 7.5 \text{ Gy}$), or 55 Gy ($5 \times 11 \text{ Gy}$), respectively. The mean differences (averaged over both fractionation schemes) between the accumulated GTV $D_{98\%}$, GTV D_{mean} , and GTV $D_{2\%}$ of S1 and S2 (0.9 Gy, 0.6 Gy, and 0.2 Gy lower for S2), and S1 and S3 (0.0 Gy, 0.5 Gy, and 1.1 Gy higher for S3) were not statistically significant. The two proton therapy scenarios achieved significant reductions in mean ipsilateral lung dose (-8% for S2; -23% for S3) and mean heart dose (-79% for S2; -83% for S3) compared to S1.

The heart and chest wall $D_{0.1\text{cc}}$ were larger for both S2 and S3 compared to S1, of which only the difference for the chest wall for S2 was significant (49.7 Gy for S1; 55.7 Gy for S2). The mean $D_{0.1\text{cc}}$ to the great vessels, esophagus, spinal cord, and trachea were smaller by up to 11.1 Gy for S2 and up to 10.4 Gy for S3 relative to S1. Due to the low number of cases, the differences for these OARs were not tested for statistical significance individually, but in a pooled analysis with 14 cases. The mean pooled $D_{0.1\text{cc}}$ for these OARs were significantly smaller by 7.0 Gy (S2; 25.6 Gy) and 6.8 Gy (S3; 25.7 Gy) compared to S1 (32.5 Gy).

The PBT $D_{0.1\text{cc}}$ was reduced from 48.1 Gy (S1) to 45.0 Gy (-6% ; $p = 0.094$) for S2 and to 39.2 Gy (-19% ; $p = 0.005$) for S3. The mean absolute volumes at all investigated dose levels were smaller for S2 and S3 compared to S1. The volume reductions were significant for all dose levels, except for the $V_{100\%}$ and $V_{80\%}$ for S2. In general, the volume reductions with respect to S1 were larger for S3 than for S2, with relative differences up to 60% ($V_{80\%}$ of 0.5 cm^3 for S1 and 0.2 cm^3 for S3).

For the pooled analysis for OARs located within 1 cm of the PTV, no significant differences of the $D_{0.1\text{cc}}$ were found. For OARs at a distance of 1–2 cm to the PTV, the $D_{0.1\text{cc}}$ were significantly smaller for S2 (reduction by

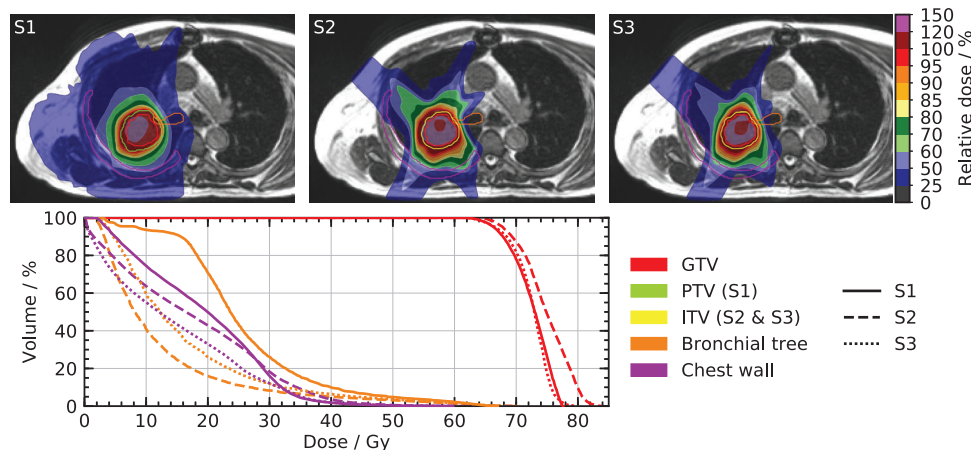


FIGURE 1 Accumulated dose distributions and DVHs. (Top): The accumulated dose distributions relative to the prescribed dose (60 Gy) for an exemplary patient (Patient 2) and the three treatment scenarios are superimposed on the planning MRI scan. (Bottom): The corresponding DVHs for the GTV and OARs located within 2 cm of the PTV (bronchial tree and chest wall) are plotted. Deviations between the GTV $D_{98\%}$ values for the three scenarios originate from the fact that the baseline plan (S2) and fractional plans (S3) were normalized to the same GTV $D_{98\%}$ with respect to S1, but the accumulated doses after dose recalculation and deformation to the planning images are shown.

19% from 30.2 to 24.6 Gy) and S3 (reduction by 24% from 30.2 to 23.1 Gy) compared to S1.

4 | DISCUSSION

This study aimed at identifying potential dosimetric benefits of today's state-of-the-art non-adaptive IMPT and future online adaptive IMPT, with respect to MRgRT, representing today's most sophisticated photon therapy treatment technique which is able to effectively account for interfractional and intrafractional changes through online plan adaptation and gated beam delivery. While online adaptive proton therapy is not clinically available yet, recent technological advancements might allow a clinical introduction in the near future.²⁸

For the central lung tumor patients included in this study, no significant differences of the $D_{0.1cc}$ to OARs within 1 cm of the PTV were observed for non-adaptive (S2) or online adaptive (S3) proton therapy compared to MRgRT (S1). In contrast, the $D_{0.1cc}$ to OARs with a distance between 1 and 2 cm to the PTV were significantly lower for both S2 and S3 compared to S1. The three treatment scenarios achieved similar target coverage, with no significant differences of the accumulated GTV $D_{98\%}$, GTV D_{mean} , and GTV $D_{2\%}$ between S1 & S2, and S1 & S3. The accumulated GTV $D_{98\%}$ was above the prescribed dose for all patients and scenarios. For S2, the lack of plan adaptation led to a slightly lower GTV $D_{98\%}$ compared to S1 and – for most cases – to higher OAR $D_{0.1cc}$ values compared to S3. For S2 and S3, fewer volume constraints were violated compared to S1 and the mean heart and lung doses were significantly reduced.

Both the maximum dose to the PBT and the bronchial volumes irradiated to high doses have been identified

as risk factors for high-grade toxicities and treatment related death.^{23,24,58,59} While no significant reductions of the PBT $D_{0.1cc}$, $V_{100\%}$, and $V_{80\%}$ for non-adaptive proton therapy (S2) compared to MRgRT (S1) were observed, our results indicate that significant and considerable relative reductions in the PBT $D_{0.1cc}$ (–19%), and the PBT volumes subjected to high doses (–60% for $V_{80\%}$), could become feasible with online adaptive IMPT (S3) in comparison to MRgRT (S1). The absolute $V_{100\%}$ and $V_{80\%}$ values and their differences among the respective treatment scenarios are only one order of magnitude larger than the dose calculation grid voxel size. Consequently, they are sensitive to dose calculation and DIR uncertainties, and their true values might differ since the impact of intrafractional motion within the gating window could not be investigated. Nevertheless, the results suggest that online adaptive IMPT could potentially reduce the rate of high-grade toxicities for central lung tumor treatments. The potential clinical impact of these PBT dose reductions cannot be reliably estimated as accurate tolerance doses for the bronchial tree are unknown for a number of reasons. For instance, the number of prospective clinical studies are limited, the fractionation schemes employed are heterogeneous, different image guidance and delivery techniques are used, and contouring of the PBT varies.^{58,59} Furthermore, most studies only reported the planned maximum PBT dose, which is not robust against interfractional and intrafractional changes, particularly in presence of the inhomogeneous dose distributions in SBRT.⁵⁸ We observed relative differences between the planned (baseline plan) and accumulated OAR $D_{0.1cc}$ parameters by up to 4% for the online adaptive treatment scenarios (S1 and S3) and up to 11% for the non-adaptive scenario (S2; Table S4). Therefore, studies comparing accumulated doses like the present

TABLE 3 DVH parameter analysis results.

Structure	n	Parameter	Unit	S1		Comparison between S1 & S2				Comparison between S1 & S3			
				S1	S2	S2-S1	p	sig. ^a	S3	S3-S1	p	sig. ^a	
GTV (8 × 7.5 Gy) ^b	13	$D_{98\%}$	Gy	66.0	64.4	-1.6	0.265		65.9	-0.1	0.495		
GTV (5 × 11 Gy) ^b	5			59.6	60.5	+0.9			59.8	+0.2			
GTV (8 × 7.5 Gy) ^b	13	D_{mean}	Gy	71.1	70.3	-0.8	0.468		72.0	+0.9	0.393		
GTV (5 × 11 Gy) ^b	5			65.6	65.4	-0.3			65.1	-0.5			
GTV (8 × 7.5 Gy) ^b	13	$D_{2\%}$	Gy	75.4	75.5	+0.0	0.981		77.2	+1.8	0.229		
GTV (5 × 11 Gy) ^b	5			70.6	69.8	-0.7			69.8	-0.7			
Lung ^c	18	D_{mean}	Gy	8.6	7.8	-0.7	0.006	*	6.6	-2.0	<0.001	*	
Heart	18	D_{mean}	Gy	4.2	1.0	-3.3	<0.001	*	0.7	-3.5	<0.001	*	
Heart	9	$D_{0.1\text{cc}}$	Gy	55.3	58.8	+3.5	0.359		57.3	+2.0	0.301		
PBT ^d	13	$D_{0.1\text{cc}}$	Gy	48.1	45.0	-3.1	0.094		39.2	-8.9	0.005	*	
PBT ^d	13	$V_{100\%}$ ^e	cm ³	0.1	0.1	-0.0	0.090		0.1	-0.0	0.018	*	
PBT ^d	13	$V_{80\%}$ ^e	cm ³	0.5	0.3	-0.2	0.051		0.2	-0.3	0.011	*	
PBT ^d	13	$V_{60\%}$ ^e	cm ³	1.1	0.7	-0.4	0.015	*	0.5	-0.6	0.008	*	
PBT ^d	13	$V_{40\%}$ ^e	cm ³	2.7	1.5	-1.2	0.006	*	1.1	-1.6	<0.001	*	
PBT ^d	13	$V_{20\%}$ ^e	cm ³	4.5	3.4	-1.2	0.033	*	2.5	-2.0	<0.001	*	
Chest wall	12	$D_{0.1\text{cc}}$	Gy	49.7	55.7	+6.0	0.003	*	51.3	+1.6	0.380		
Great vessels ^f	5	$D_{0.1\text{cc}}$	Gy	41.8	37.6	-4.2			37.6	-4.2			
Esophagus ^f	4	$D_{0.1\text{cc}}$	Gy	30.0	19.0	-11.1	0.002	*	19.7	-10.4	0.002	*	
Spinal cord ^f	3	$D_{0.1\text{cc}}$	Gy	18.9	12.4	-6.5			14.4	-4.6			
Trachea ^f	2	$D_{0.1\text{cc}}$	Gy	34.8	28.3	-6.5			25.2	-9.6			
OAR < 1 cm ^g	34	$D_{0.1\text{cc}}$	Gy	51.5	52.9	+1.3	0.388		49.4	-2.1	0.222		
1 cm < OAR < 2 cm ^h	14	$D_{0.1\text{cc}}$	Gy	30.2	24.6	-5.6	0.049	*	23.1	-7.2	0.007	*	

Notes: The mean DVH parameters of the accumulated physical doses (S1) or relative biologically effective (RBE) doses (S2 and S3; RBE = 1.1) are reported. Differences between S1 and S2, as well as S1 and S3 were compared in a pair-wise two-tailed Wilcoxon signed rank test, where differences were considered to be statistically significant for a p -value < 0.05.

^aSignificance of difference ($p < 0.05$) is indicated by an asterisk (*).

^bMean values are reported for the two fractionation schemes separately, but Wilcoxon signed-rank test was conducted for both fractionation schemes combined.

^cIpsilateral lung excluding GTV.

^dProximal bronchial tree; up to second bifurcation.

^eVolume at dose; relative to prescribed dose.

^fNo statistical analysis was performed individually due to low number of cases, but $D_{0.1\text{cc}}$ values for the great vessels, esophagus, spinal cord, and trachea were pooled before statistical testing.

^gDistance between PTV and OAR below 1 cm.

^hDistance between PTV and OAR between 1 and 2 cm.

work could help to determine tolerance doses to the PBT more accurately,⁵⁸ when correlated with clinical outcome data.⁶⁰ This would allow a quantification of the potential clinical benefit of online adaptive IMPT compared to MRgRT.

Few planning studies⁵⁷ and one randomized phase 2 clinical trial¹⁰ have compared photon and proton therapy for central lung tumors. Register et al.⁵⁷ conducted a plan comparison study including 15 patients between photon SBRT, passive-scattering proton therapy, and IMPT and evaluated the lung dose and the maximum dose to OARs within 2 cm of the PTV. More recently, Bayasgalan et al.⁶¹ compared passive-scattering proton therapy to different photon therapy delivery techniques, including IMRT for 42 lung cancer patients, thereof eleven with central lung tumors. The findings of these reports cannot be directly compared to the results of our study, since

different margin concepts, image guidance and delivery techniques were used, and only the planned dose and not the accumulated doses were reported. Nevertheless, the main findings of these studies and our work were similar, concluding that proton therapy can achieve significant mean dose sparing to the heart and lungs and lower the maximum dose to OARs within 2 cm of the target.

Our study shows that gated proton therapy with or without daily plan adaptations achieves $D_{0.1\text{cc}}$ reductions to OARs in close, but not in direct proximity to the PTV with respect to MRgRT. This is likely a result of partial volume overlaps of OARs with the target volumes, and the chosen positional and range robustness settings. Our findings are consistent with a study by Seco et al.,⁶² who compared photon and proton SBRT with passive-scattering proton beams for ten peripheral

lung cancer patients. The authors found that OARs in vicinity of the target volume received higher doses for proton compared to photon SBRT and attributed this to larger high-dose regions due to range uncertainties in proton therapy. Consequently, reduction in proton range uncertainties, for example, by using a dual-energy CT scan,⁶³ could further increase this dosimetric benefit of non-adaptive and online adaptive IMPT over MRgRT.

The vCT images used for dose calculation for all three treatment scenarios were automatically generated by the MRIdian treatment planning system by deformably registering the planning CT image to the baseline MRI and fractional MRI scans. This method can yield inaccurate results in case of pronounced anatomical changes such as differences in lung density induced by pleural effusion or atelectasis. Such changes could be detected and compensated for in the online adaptive scenarios (S1 and S3) by acquiring in-room CT images or using more sophisticated synthetic CT generation methods. For non-adaptive proton therapy (S2), these changes could introduce larger deviations from the planned dose distributions, and the dosimetric benefit compared to S1 could be smaller in such clinical situations.

While the robustness settings for S2 were chosen based on a published protocol,⁵⁴ assumptions had to be made for S3 as this technique is not yet in clinical use. To enable a fair comparison, similar residual uncertainties were assumed for the two online adaptive scenarios. Interfractional anatomical changes can be detected and compensated for through plan adaptation in S3 while they have to be prospectively accounted for in the treatment planning process in S2, justifying the different robustness settings in the two treatment scenarios. The main focus of the analyses was a comparison between the OAR doses in the different treatment scenarios. The treatment plans in S2 and S3 were normalized with respect to the GTV $D_{98\%}$ in S1 to achieve similar dose levels in the target to improve the comparability between the scenarios. On average, the (mean $\pm 1\sigma$) normalization scaling factor was (+3.1 \pm 5.4)% for S2 and (+1.6 \pm 4.5)% for S3. As a consequence, for a subset of patients with negative scaling factors (4 cases for S2; 5 cases for S3), the target coverage robustness of the scaled proton therapy plans was lowered while on average the mean OAR doses were slightly larger than necessary.

Gating within an isotropic gating window of 3 mm was assumed for all three scenarios, to focus the analyses on the impact of interfractional changes on the accumulated dose distributions in the presence or absence of online plan adaptations. While respiratory gating is not yet standard clinical practice in proton therapy today, it has been successfully clinically implemented by several centers for the treatment of lung tumors.^{49–52} In this study, the dosimetric effect of residual motion within the gating window and potential interplay effects could not be quantified since this would require – in addition to linac or proton therapy log files – time-resolved

volumetric CT imaging data acquired during treatment, which are neither available for MRgRT¹⁷ nor for proton therapy^{11,33} today. While the target coverage for the online adaptive treatment scenarios (S1 and S3) is likely robust against motion within the gating window by plan design, it is not clear whether this would also be the case for the non-adaptive scenario (S2) and needs further investigation. Interplay effects are expected to be negligible for gated MRgRT⁶⁴ and gated pencil beam delivery in IMPT, particularly when combined with further motion mitigation techniques like rescanning and enlarged spot sizes,^{53,54,65} and when the accumulated dose over all fractions is considered.

Some other study limitations must be kept in mind. Photon and proton therapy planning was performed at two different institutions by different planners and with the use of different TPSs, and proton therapy planning was done with prior knowledge of the dose distributions delivered in MRgRT. This could have led to different treatment planning strategies and priorities with respect to dose conformality and OAR sparing. Plan adaptations in S1 had to be performed online with the patient lying on the couch while there were no time restrictions for the plan adaptations for S3. To counteract this potential bias, we implemented an automated plan adaptation pipeline for S3 and kept the beam angles and planning objectives fixed with respect to the baseline plan (similar to plan adaptations in MRgRT). The ipsilateral arm was not always positioned above the head during MRgRT delivery, which led to limited proton beam angle options for some patients. Furthermore, no special attention was paid to the reproducibility of the patient body outline during MRgRT, while this is crucial and typically done in proton therapy. These limitations might bias the results and lead to suboptimal dose distributions for S2 and S3. A total of 45 (S2) or 21 (S3) setup and range error scenarios were considered during robust treatment plan optimization for the proton therapy scenarios. Only the dose distributions in the nominal scenario (i.e., no positional shifts or density scaling) for each fraction were considered for dose accumulation on the baseline vCT images. Analyzing all possible combinations of setup and range error scenarios for all treatment fractions would result in up to 10^{13} different accumulated dose distributions, and was thus beyond the scope of this study. Lastly, the DIR is directly impacting the accumulated dose distributions.⁵⁶ We paid great attention to the optimization of the DIR settings to achieve high accuracy in the target region and its proximity. When testing different settings for the controlling and focus ROIs in the hybrid intensity-based DIR, we only observed minor differences of the accumulated DVH parameters, which indicates robustness of the used DIR settings and the obtained results. Furthermore, the observed small interfractional GTV changes suggest that the effect of anatomical changes on the dose accumulation accuracy was small.

5 | CONCLUSIONS

We did not observe significant differences of the $D_{0,1cc}$ to OARs within 1 cm of the PTV between online adaptive MRgRT, non-adaptive gated proton therapy, and online adaptive proton therapy of central lung tumor patients. For OARs located at a distance of 1–2 cm of the PTV, both non-adaptive and online adaptive proton therapy achieved significantly lower $D_{0,1cc}$ values. The reduced doses to the bronchial tree in online adaptive proton therapy could potentially lead to reduced rates of high-grade toxicities in the treatment of central lung tumors, should this treatment technique become clinically available in the future. Dose accumulation studies like ours that leverage the daily imaging data acquired during MR-guided radiotherapy could help to determine OAR tolerance doses more accurately.

ACKNOWLEDGMENTS

Moritz Rabe is supported by the German Research Foundation (DFG) within the Research Training Group GRK 2274 “Advanced Medical Physics for Image-Guided Cancer Therapy.” Chukwuka Eze received funding in form of a research grant from the German Cancer Aid (Mildred Scheel-Stipendienprogramm für Krebsforschung, 2018 (57468956)).

Open access funding enabled and organized by Projekt DEAL.

CONFLICTS OF INTEREST STATEMENT


The Department of Radiation Oncology of the University Hospital of LMU Munich has research agreements with ViewRay Inc., Elekta, Brainlab, and C-RAD. The Department of Radiation Oncology at the Amsterdam University Medical Center has funded research agreements with ViewRay Inc. and Varian Medical Systems. ViewRay Inc. did not fund this study and was not involved and had no influence on the study design, the collection or analysis of data, or on the writing of the manuscript. MP reports consulting fees and honoraria from ViewRay Inc. outside of the submitted work. CB reports honoraria from ViewRay Inc., Elekta, Opasca, and C-RAD outside of the submitted work. SS serves in advisory boards for ViewRay Inc. and Varian Medical Systems outside of the submitted work.

DATA AVAILABILITY STATEMENT


Authors are not able to share data at this time.

ORCID

Moritz Rabe  <https://orcid.org/0000-0002-7085-4066>

Chukwuka Eze 

<https://orcid.org/0000-0003-3779-1398>

Suresh Senan 

<https://orcid.org/0000-0003-3995-2204>

REFERENCES

1. Timmerman R, McGarry R, Yiannoutsos C, et al. Excessive toxicity when treating central tumors in a phase II study of stereotactic body radiation therapy for medically inoperable early-stage lung cancer. *J Clin Oncol*. 2006;24(30):4833-4839. doi:10.1200/JCO.2006.07.5937
2. Chang JY, Balter PA, Dong L, et al. Stereotactic body radiation therapy in centrally and superiorly located stage I or isolated recurrent non-small-cell lung cancer. *Int J Radiat Oncol Biol Phys*. 2008;72(4):967-971. doi:10.1016/j.ijrobp.2008.08.001
3. Roach MC, Robinson CG, DeWees TA, et al. Stereotactic body radiation therapy for central early-stage NSCLC: results of a prospective phase I/II trial. *J Thorac Oncol*. 2018;13(11):1727-1732. doi:10.1016/j.jtho.2018.07.017
4. Bezjak A, Paulus R, Gaspar LE, et al. Safety and efficacy of a five-fraction stereotactic body radiotherapy schedule for centrally located non-small-cell lung cancer: NRG oncology/RTOG 0813 trial. *J Clin Oncol*. 2019;37(15):1316-1325. doi:10.1200/JCO.18.00622
5. Lindberg K, Grozman V, Karlsson K, et al. The HILUS-trial-a prospective Nordic multicenter phase 2 study of ultracentral lung tumors treated with stereotactic body radiotherapy. *J Thorac Oncol*. 2021;16(7):1200-1210. doi:10.1016/j.jtho.2021.03.019
6. Bush DA, Cheek G, Zaheer S, et al. High-dose hypofractionated proton beam radiation therapy is safe and effective for central and peripheral early-stage non-small cell lung cancer: results of a 12-year experience at Loma Linda University Medical Center. *Int J Radiat Oncol Biol Phys*. 2013;86(5):964-968. doi:10.1016/j.ijrobp.2013.05.002
7. Ono T, Yabuuchi T, Nakamura T, et al. High dose hypofractionated proton beam therapy is a safe and feasible treatment for central lung cancer. *Radiol Oncol*. 2017;51(3):324-330. doi:10.1515/raon-2017-0023
8. Nakamura N, Hotta K, Zenda S, et al. Hypofractionated proton beam therapy for centrally located lung cancer. *J Med Imaging Radiat Oncol*. 2019;63(4):552-556. doi:10.1111/1754-9485.12901
9. Kharod SM, Nichols RC, Henderson RH, et al. Image-guided hypofractionated double-scattering proton therapy in the management of centrally-located early-stage non-small cell lung cancer. *Acta Oncol*. 2020;59(10):1164-1170. doi:10.1080/0284186X.2020.1759821
10. Nantavithya C, Gomez DR, Wei X, et al. Phase 2 study of stereotactic body radiation therapy and stereotactic body proton therapy for high-risk, medically inoperable, early-stage non-small cell lung cancer. *Int J Radiat Oncol Biol Phys*. 2018;101(3):558-563. doi:10.1016/j.ijrobp.2018.02.022
11. Landry G, Hua CH. Current state and future applications of radiological image guidance for particle therapy. *Med Phys*. 2018;45(11):e1086-e1095. doi:10.1002/mp.12744
12. Acharya S, Fischer-Valuck BW, Kashani R, et al. Online magnetic resonance image guided adaptive radiation therapy: first clinical applications. *Int J Radiat Oncol Biol Phys*. 2016;94(2):394-403. doi:10.1016/j.ijrobp.2015.10.015
13. Raaymakers BW, Jurgenliemk-Schulz IM, Bol GH, et al. First patients treated with a 1.5 T MRI-Linac: clinical proof of concept of a high-precision, high-field MRI guided radiotherapy treatment. *Phys Med Biol*. 2017;62(23):L41-L50. doi:10.1088/1361-6560/aa9517
14. van Sornsens de Koste JR, Palacios MA, Bruynzeel AME, Slotman BJ, Senan S, Lagerwaard FJ. MR-guided gated stereotactic radiation therapy delivery for lung, adrenal, and pancreatic tumors: a geometric analysis. *Int J Radiat Oncol Biol Phys*. 2018;102(4):858-866. doi:10.1016/j.ijrobp.2018.05.048
15. Corradini S, Alongi F, Andratschke N, et al. MR-guidance in clinical reality: current treatment challenges and future perspectives. *Radiat Oncol*. 2019;14(92):1-12. doi:10.1186/s13014-019-1308-y

16. Mucic S, Dempsey JF. The ViewRay system: magnetic resonance-guided and controlled radiotherapy. *Semin Radiat Oncol*. 2014;24(3):196-199. doi:10.1016/j.semradonc.2014.02.008
17. Kurz C, Buizza G, Landry G, et al. Medical physics challenges in clinical MR-guided radiotherapy. *Radiat Oncol*. 2020;15(93):1-16. doi:10.1186/s13014-020-01524-4
18. Finazzi T, Haasbeek CJA, Spoelstra FOB, et al. Clinical outcomes of stereotactic MR-guided adaptive radiation therapy for high-risk lung tumors. *Int J Radiat Oncol Biol Phys*. 2020;107(2):270-278. doi:10.1016/j.ijrobp.2020.02.025
19. Finazzi T, Palacios MA, Spoelstra FOB, et al. Role of on-table plan adaptation in MR-guided ablative radiation therapy for central lung tumors. *Int J Radiat Oncol Biol Phys*. 2019;104(4):933-941. doi:10.1016/j.ijrobp.2019.03.035
20. Regnery S, Buchele C, Weykamp F, et al. Adaptive MR-guided stereotactic radiotherapy is beneficial for ablative treatment of lung tumors in high-risk locations. *Front Oncol*. 2022;11:757031. doi:10.3389/fonc.2021.757031
21. Henke LE, Olsen JR, Contreras JA, et al. Stereotactic MR-Guided Online Adaptive Radiation Therapy (SMART) for ultracentral thorax malignancies: results of a phase 1 trial. *Adv Radiat Oncol*. 2019;4(1):201-209. doi:10.1016/j.adro.2018.10.003
22. Haseltine JM, Rimmer A, Gelblum DY, et al. Fatal complications after stereotactic body radiation therapy for central lung tumors abutting the proximal bronchial tree. *Pract Radiat Oncol*. 2016;6(2):e27-33. doi:10.1016/j.ppro.2015.09.012
23. Duijm M, Schillemans W, Aerts JG, Heijmen B, Nuytens JJ. Dose and volume of the irradiated main bronchi and related side effects in the treatment of central lung tumors with stereotactic radiotherapy. *Semin Radiat Oncol*. 2016;26(2):140-148. doi:10.1016/j.semradonc.2015.11.002
24. Tekatli H, Duijm M, Oomen-de Hoop E, et al. Normal tissue complication probability modeling of pulmonary toxicity after stereotactic and hypofractionated radiation therapy for central lung tumors. *Int J Radiat Oncol Biol Phys*. 2018;100(3):738-747. doi:10.1016/j.ijrobp.2017.11.022
25. Unkelbach J, Paganetti H. Robust proton treatment planning: physical and biological optimization. *Semin Radiat Oncol*. 2018;28(2):88-96. doi:10.1016/j.semradonc.2017.11.005
26. Chang JY, Li H, Zhu XR, et al. Clinical implementation of intensity modulated proton therapy for thoracic malignancies. *Int J Radiat Oncol Biol Phys*. 2014;90(4):809-818. doi:10.1016/j.ijrobp.2014.07.045
27. Placidi L, Bolsi A, Lomax AJ, et al. Effect of anatomic changes on pencil beam scanned proton dose distributions for cranial and extracranial tumors. *Int J Radiat Oncol Biol Phys*. 2017;97(3):616-623. doi:10.1016/j.ijrobp.2016.11.013
28. Albertini F, Matter M, Nenoff L, Zhang Y, Lomax A. Online daily adaptive proton therapy. *Br J Radiol*. 2020;93(1107):20190594. doi:10.1259/bjr.20190594
29. Paganetti H, Botas P, Sharp GC, Winey B. Adaptive proton therapy. *Phys Med Biol*. 2021;66(22):22TR01. doi:10.1088/1361-6560/ac344f
30. Nenoff L, Matter M, Charmillot M, et al. Experimental validation of daily adaptive proton therapy. *Phys Med Biol*. 2021;66(20):205010. doi:10.1088/1361-6560/ac2b84
31. Sun B, Yang D, Lam D, et al. Toward adaptive proton therapy guided with a mobile helical CT scanner. *Radiother Oncol*. 2018;129(3):479-485. doi:10.1016/j.radonc.2018.08.021
32. Oliver JA, Zeidan O, Meeks SL, et al. Commissioning an in-room mobile CT for adaptive proton therapy with a compact proton system. *J Appl Clin Med Phys*. 2018;19(3):149-158. doi:10.1002/acm2.12319
33. Schmitz H, Rabe M, Janssens G, et al. Validation of proton dose calculation on scatter corrected 4D cone beam computed tomography using a porcine lung phantom. *Phys Med Biol*. 2021;66(17):175022. doi:10.1088/1361-6560/ac16e9
34. Kurz C, Dedes G, Resch A, et al. Comparing cone-beam CT intensity correction methods for dose recalculation in adaptive intensity-modulated photon and proton therapy for head and neck cancer. *Acta Oncol*. 2015;54(9):1651-1657. doi:10.3109/0284186X.2015.1061206
35. Hansen DC, Landry G, Kamp F, et al. ScatterNet: a convolutional neural network for cone-beam CT intensity correction. *Med Phys*. 2018;45(11):4916-4926. doi:10.1002/mp.13175
36. Hoffmann A, Oborn B, Moteabbed M, et al. MR-guided proton therapy: a review and a preview. *Radiat Oncol*. 2020;15(1):129. doi:10.1186/s13014-020-01571-x
37. Pham TT, Whelan B, Oborn BM, et al. Magnetic resonance imaging (MRI) guided proton therapy: a review of the clinical challenges, potential benefits and pathway to implementation. *Radiother Oncol*. 2022;170:37-47. doi:10.1016/j.radonc.2022.02.031
38. Raaymakers BW, Raaijmakers AJ, Lagendijk JJ. Feasibility of MRI guided proton therapy: magnetic field dose effects. *Phys Med Biol*. 2008;53(20):5615-5622. doi:10.1088/0031-9155/53/20/003
39. Kurz C, Landry G, Resch AF, et al. A Monte-Carlo study to assess the effect of 1.5 T magnetic fields on the overall robustness of pencil-beam scanning proton radiotherapy plans for prostate cancer. *Phys Med Biol*. 2017;62(21):8470-8482. doi:10.1088/1361-6560/aa8de9
40. Schellhammer SM, Hoffmann AL, Gantz S, et al. Integrating a low-field open MR scanner with a static proton research beam line: proof of concept. *Phys Med Biol*. 2018;63(23):23LT01. doi:10.1088/1361-6560/aaece8
41. Spadea MF, Maspero M, Zaffino P, Seco J. Deep learning based synthetic-CT generation in radiotherapy and PET: a review. *Med Phys*. 2021;48(11):6537-6566. doi:10.1002/mp.15150
42. Thummerer A, Zaffino P, Meijers A, et al. Comparison of CBCT based synthetic CT methods suitable for proton dose calculations in adaptive proton therapy. *Phys Med Biol*. 2020;65(9):095002. doi:10.1088/1361-6560/ab7d54
43. Kawula M, Purice D, Li M, et al. Dosimetric impact of deep learning-based CT auto-segmentation on radiation therapy treatment planning for prostate cancer. *Radiat Oncol*. 2022;17(1):21. doi:10.1186/s13014-022-01985-9
44. Klüter S. Technical design and concept of a 0.35 T MR-Linac. *Clin Transl Radiat Oncol*. 2019;18:98-101. doi:10.1016/j.ctro.2019.04.007
45. Chang JY, Bezjak A, Mornex F, Committee IART. Stereotactic ablative radiotherapy for centrally located early stage non-small-cell lung cancer: what we have learned. *J Thorac Oncol*. 2015;10(4):577-585. doi:10.1097/JTO.0000000000000453
46. Tekatli H, Haasbeek N, Dahele M, et al. Outcomes of hypofractionated high-dose radiotherapy in poor-risk patients with "Ultracentral" non-small cell lung cancer. *J Thorac Oncol*. 2016;11(7):1081-1089. doi:10.1016/j.jtho.2016.03.008
47. Bohoudi O, Bruynzeel AME, Senan S, et al. Fast and robust online adaptive planning in stereotactic MR-guided adaptive radiation therapy (SMART) for pancreatic cancer. *Radiother Oncol*. 2017;125(3):439-444. doi:10.1016/j.radonc.2017.07.028
48. Benedict SH, Yenice KM, Followill D, et al. Stereotactic body radiation therapy: the report of AAPM Task Group 101. *Med Phys*. 2010;37(8):4078-4101. doi:10.1118/1.3438081
49. Nakajima K, Iwata H, Ogino H, et al. Clinical outcomes of image-guided proton therapy for histologically confirmed stage I non-small cell lung cancer. *Radiat Oncol*. 2018;13(1):199. doi:10.1186/s13014-018-1144-5
50. Gelover E, Deisher AJ, Herman MG, Johnson JE, Kruse JJ, Tryggstad EJ. Clinical implementation of respiratory-gated spot-scanning proton therapy: an efficiency analysis of active motion management. *J Appl Clin Med Phys*. 2019;20(5):99-108. doi:10.1002/acm2.12584

51. Yoshimura T, Shimizu S, Hashimoto T, et al. Analysis of treatment process time for real-time-image gated-spot-scanning proton-beam therapy (RGPT) system. *J Appl Clin Med Phys*. 2020;21(2):38-49. doi:10.1002/acm2.12804
52. Fattori G, Hrbacek J, Regele H, et al. Commissioning and quality assurance of a novel solution for respiratory-gated PBS proton therapy based on optical tracking of surface markers. *Z Med Phys*. 2022;32(1):52-62. doi:10.1016/j.zemedi.2020.07.001
53. Gut P, Krieger M, Lomax T, Weber DC, Hrbacek J. Combining rescanning and gating for a time-efficient treatment of mobile tumors using pencil beam scanning proton therapy. *Radiother Oncol*. 2021;160:82-89. doi:10.1016/j.radonc.2021.03.041
54. Meijers A, Knopf AC, Crijns APG, et al. Evaluation of interplay and organ motion effects by means of 4D dose reconstruction and accumulation. *Radiother Oncol*. 2020;150:268-274. doi:10.1016/j.radonc.2020.07.055
55. Weistrand O, Svensson S. The ANACONDA algorithm for deformable image registration in radiotherapy. *Med Phys*. 2015;42(1):40-53. doi:10.1118/1.4894702
56. Brock KK, Mutic S, McNutt TR, Li H, Kessler ML. Use of image registration and fusion algorithms and techniques in radiotherapy: Report of the AAPM Radiation Therapy Committee Task Group No. 132. *Med Phys*. 2017;44(7):e43-e76. doi:10.1002/mp.12256
57. Register SP, Zhang X, Mohan R, Chang JY. Proton stereotactic body radiation therapy for clinically challenging cases of centrally and superiorly located stage I non-small-cell lung cancer. *Int J Radiat Oncol Biol Phys*. 2011;80(4):1015-1022. doi:10.1016/j.ijrobp.2010.03.012
58. Lindberg K, Onjukka E. Medical consequences of radiation exposure of the bronchi-what can we learn from high-dose precision radiation therapy? *J Radiol Prot*. 2021;41(4):S355-S370. doi:10.1088/1361-6498/ac28ef
59. Tekatli H, Spoelstra FOB, Palacios M, van Sornsen de Koste J, Slotman BJ, Senan S. Stereotactic ablative radiotherapy (SABR) for early-stage central lung tumors: new insights and approaches. *Lung Cancer*. 2018;123:142-148. doi:10.1016/j.lungcan.2018.07.002
60. Jaffray DA, Lindsay PE, Brock KK, Deasy JO, Tome WA. Accurate accumulation of dose for improved understanding of radiation effects in normal tissue. *Int J Radiat Oncol Biol Phys*. 2010;76(3 Suppl):S135-139. doi:10.1016/j.ijrobp.2009.06.093
61. Bayasgalan U, Moon SH, Kim TH, Kim TY, Lee SH, Suh YG. Dosimetric comparisons between proton beam therapy and modern photon radiation techniques for stage I non-small cell lung cancer according to tumor location. *Cancers*. 2021;13(24):6356. doi:10.3390/cancers13246356
62. Seco J, Panahandeh HR, Westover K, Adams J, Willers H. Treatment of non-small cell lung cancer patients with proton beam-based stereotactic body radiotherapy: dosimetric comparison with photon plans highlights importance of range uncertainty. *Int J Radiat Oncol Biol Phys*. 2012;83(1):354-361. doi:10.1016/j.ijrobp.2011.05.062
63. Peters N, Wohlfahrt P, Hofmann C, et al. Reduction of clinical safety margins in proton therapy enabled by the clinical implementation of dual-energy CT for direct stopping-power prediction. *Radiother Oncol*. 2022;166:71-78. doi:10.1016/j.radonc.2021.11.002
64. Ehrbar S, Braga Kaser S, Chamberlain M, et al. MR-guided beam gating: residual motion, gating efficiency and dose reconstruction for stereotactic treatments of the liver and lung. *Radiother Oncol*. 2022;174:101-108. doi:10.1016/j.radonc.2022.07.007
65. Grassberger C, Dowdell S, Sharp G, Paganetti H. Motion mitigation for lung cancer patients treated with active scanning proton therapy. *Med Phys*. 2015;42(5):2462-2469. doi:10.1118/1.4916662

SUPPORTING INFORMATION

Additional supporting information can be found online in the Supporting Information section at the end of this article.

How to cite this article: Rabe M, Palacios MA, van Sörnsen de Koste JR, et al. Comparison of MR-guided radiotherapy accumulated doses for central lung tumors with non-adaptive and online adaptive proton therapy. *Med Phys*. 2023;50:2625–2636. <https://doi.org/10.1002/mp.16319>